2012

# Optimization of Peripheral Finned-Tube Evaporators Using Entropy Generation Minimization

Bruno Pussoli
jrb@polo.ufsc.br

Jader Barbosa Jr.

Luciana da Silva

Massoud Kaviany

# Optimization of Peripheral Finned-Tube Evaporators Using Entropy Generation Minimization

Bruno PUSSOLI[1], Jader BARBOSA Jr.[1]*, Luciana DA SILVA[2], Massoud KAVIANY[3]

[1]Federal University of Santa Catarina, Department of Mechanical Engineering,
Florianópolis, SC, Brazil
* Corresponding Author. E-mail: jrb@polo.ufsc.br

[2]Embraco Compressors,
Joinville, SC, Brazil

[3]University of Michigan, Department of Mechanical Engineering,
Ann Arbor, MI, USA

## ABSTRACT

The peripheral finned-tube (PFT) is a new geometry for enhanced air-side heat transfer under moisture condensate blockage (evaporators). It consists of individual hexagonal (peripheral) fin arrangements with radial fins whose bases are attached to the tubes and tips are interconnected with the peripheral fins. In this paper, experimentally validated semi-empirical models for the air-side heat transfer and pressure drop are combined with the entropy generation minimization theory to determine the optimal characteristics of PFT heat exchangers. The analysis is based on three independent parameters, i.e., porosity, equivalent particle diameter and particle-based Reynolds number. The total heat transfer rate is a fixed constraint. The optimal heat exchanger configurations, i.e., those in which the entropy generation number reaches a minimum, are calculated for constant heat flux and constant tube wall temperature boundary conditions. Performance evaluation criteria of fixed geometry, fixed face area and variable geometry were implemented. In all cases, it was possible to determine a combination of independent parameters that provided a minimum entropy generation rate.

## 1. INTRODUCTION

Finned-tube heat exchangers are encountered in the majority of direct expansion vapor compression refrigeration applications. With the aim of increasing the air-side thermal conductance to meet space (volume) restrictions and pumping power constraints, a number of extended surface types have been proposed and reviewed in the literature (Wang, 2000; 2010).

Wu *et al.* (2007) proposed an extended surface geometry for enhanced performance under dehumidifying conditions. The peripheral finned-tube (PFT) geometry shown in Fig. 1 is a cross-flow configuration in which the air-side is composed by hexagonal arrangements of open-pore cells formed by six radial fins whose bases are attached to the tubes and tips are connected to six peripheral fins (Fig. 2). The finned surface is composed of three levels of fin arrangement, each characterized by the length of radial fin and mounted with a 30° offset from its neighbouring level. Pussoli *et al.* (2012) carried out an experimental evaluation of the PFT heat exchanger performance. Five prototypes with different values of radial fin length, fin thickness, heat exchanger flow length, face area, and fin distribution were tested in a wind-tunnel calorimeter for air superficial velocities between 0.84 and 4.11 m/s. The heat transfer and pressure drop data were predicted by a 1-D model based on the theory of porous media that accounted for the heat transfer by conduction in the fins. The model incorporated correlations for the interstitial Nusselt number and friction factor in the determination of the heat transfer rate and pressure drop.

The optimum geometric configuration of a given heat exchanger can be achieved in a number of ways. Shah and Sekulic (2003) and Webb and Kim (2005) presented general overviews of performance evaluation criteria (PEC) for heat transfer surfaces and heat exchangers with and without phase change. Yilmaz *et al.* (2005) and Yilmaz *et al.* (2001) reviewed the existing 1st and 2nd-law based PEC, respectively. 2nd-law-based PEC are generally formulated so as to achieve a minimum entropy generation (or a minimum exergy destruction) in a particular application. Hesselgreaves (2000) reviewed several 2nd-law-based approaches of PEC and presented a rational calculation method by deriving new relations for the local rate generation process and for the nearly-balanced counterflow arrangement. Zimparov (2000, 2001) developed extended PEC for enhanced heat transfer surfaces based on the entropy production theorem so as to include the effect of fluid temperature variation in a tubular heat exchanger.

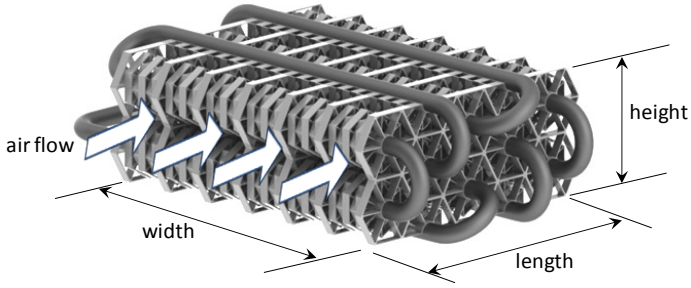


**Figure 1:** The peripheral finned-tube geometry (Pussoli *et al.*, 2012).

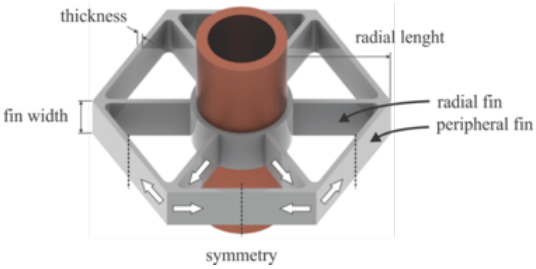


**Figure 2:** Fin geometric parameters.

The purpose of this paper is to combine the experimentally validated modeling framework of Pussoli *et al.* (2012) for the air-side heat transfer and pressure drop with the entropy generation minimization (EGM) theory of Bejan (1982) to determine the optimum characteristics of PFT heat exchangers. The fixed geometry, fixed face area and variable geometry performance evaluation criteria (PEC) of Webb and Kim (2005) were applied for boundary conditions of prescribed wall temperature and wall heat flux. In all situations, it was possible to determine a combination of independent parameters that provided a minimum entropy generation rate.

## 2. MODELING

For high absolute temperature flows, the entropy generation rate per unit length in a heat exchanger can be computed through the following equation (Bejan, 1982)

$$\dot{S}'_{gen} = \dot{S}'_{gen,\Delta T} + \dot{S}'_{gen,\Delta P} = \frac{q'\left(T_w - T_a\right)}{T_a^2} + \frac{\dot{m}_a}{\rho_a T_a}\left(-\frac{dP}{dx}\right) \tag{1}$$

where the first term is associated with the generation of entropy due to heat transfer across a finite temperature difference and the second is due to fluid friction. In the PFT geometry, due to the large number of geometric variables involved (three levels of radial fin length, thickness and width) the optimization was carried out in terms of three dimensionless parameters, namely, porosity, particle Reynolds number and equivalent particle diameter. The two fundamental boundary conditions of constant wall temperature and wall heat flux were evaluated.

### 2.1 Constant Wall Temperature

This limiting case approximates to that of an evaporator with a negligible combined thermal resistance of internal convection and wall conduction. The first term on the right of eq. (1) can be replaced by

$$\dot{S}'_{gen,\Delta T} = \eta_0 \bar{h} \frac{\left(T_w - T_a\right)^2}{T_a^2} \frac{dA}{dx} \tag{2}$$

where the air-side heat transfer coefficient is given by

$$\bar{h} = \frac{\dot{m}_a c_{pa} \mathrm{St}}{A_c \varepsilon} = \frac{\dot{m}_a c_{pa}}{A_c \varepsilon} \frac{\mathrm{Nu}_{Dp}}{\mathrm{Re}_{Dp} \mathrm{Pr}} \tag{3}$$

and the rate of change of the surface area with distance can be calculated as

$$\frac{dA}{dx} = \frac{dA}{dV_s} \frac{dV_s}{dV} = \frac{6}{D_p} \left(1-\varepsilon\right) \tag{4}$$

The pressure gradient in the porous medium can be calculated as follows (Kaviany, 2011)

$$-\frac{dP}{dx} = f \frac{\rho U_D^2}{D_p} \frac{\left(1-\varepsilon\right)}{\varepsilon^3} \tag{5}$$

Therefore, in dimensionless form, eq. (1) can be written in terms of the entropy generation number as follows

$$\frac{dN_S}{dx} = \frac{d}{dx}\left(\frac{\dot{S}_{gen}}{\dot{m}_a c_{pa}}\right) = \eta_0 \frac{6\mathrm{St}}{D_p} \frac{\left(1-\varepsilon\right)}{\varepsilon} \frac{\left(T_w - T_a\right)^2}{T_a^2} + f \frac{\mathrm{Re}_{Dp}^2 \nu_a^2}{D_p^3 c_{p,a} T_a} \frac{\left(1-\varepsilon\right)^3}{\varepsilon^3} \tag{6}$$

Assuming that the overall surface efficiency and the physical properties remain constant (they were estimated at the log-mean temperature between the inlet and outlet), the air-side entropy generation number for the heat exchanger (the objective function in the optimization) is given by

$$N_S = \eta_0 \frac{6\mathrm{St}}{D_p} \frac{\left(1-\varepsilon\right)}{\varepsilon} \int_0^L \frac{\left(T_w - T_a\right)^2}{T_a^2} dx + f \frac{\mathrm{Re}_{Dp}^2 \nu_a^2}{D_p^3 c_{p,a}} \frac{\left(1-\varepsilon\right)^3}{\varepsilon^3} \int_0^L \frac{1}{T_a} dx \tag{7}$$

where the air temperature distribution is given by

$$\frac{T_w - T_a}{T_w - T_{a,in}} = \exp\left[-\left(\frac{\eta_0 \bar{h} A}{\dot{m}_a c_{pa}}\right)\frac{x}{L}\right] \tag{8}$$

### 2.2 Constant Heat Flux

This case approximates to that of a balanced heat exchanger, i.e., one in which the thermal capacity rates of both streams are identical. The rate of entropy generation due to heat transfer is written in the form (Bejan, 1982)

$$\dot{S}'_{gen,\Delta T} = \frac{q''^2}{\eta_o \bar{h} T_a^2} \frac{dA}{dx} \tag{9}$$

where the heat flux is computed as the ratio of the heat transfer rate (a fixed constraint in the analysis) and the air-side surface area. After an algebraic manipulation of eqs. (1) and (9), with the friction term identical to that in eq. (6), the following relationship can be obtained for the rate of change of the entropy generation number

$$\frac{dN_S}{dx} = \frac{6q''^2 D_p \varepsilon}{\eta_0 \Pr^2 k_a^2 T_a^2 \mathrm{St}\left(1-\varepsilon\right)\mathrm{Re}_{Dp}^2} + f\frac{\mathrm{Re}_{Dp}^2 \nu_a^2}{D_p^3 c_{p,a} T_a}\frac{\left(1-\varepsilon\right)^3}{\varepsilon^3} \tag{10}$$

Again, assuming constant physical properties and overall surface efficiency, one has

$$N_S = \frac{6q''^2 D_p \varepsilon}{\eta_0 \Pr^2 k_a^2 \mathrm{St}\left(1-\varepsilon\right)\mathrm{Re}_{Dp}^2}\int_0^L \frac{1}{T_a^2}dx + f\frac{\mathrm{Re}_{Dp}^2 \nu_a^2}{D_p^3 c_{p,a}}\frac{\left(1-\varepsilon\right)^3}{\varepsilon^3}\int_0^L \frac{1}{T_a}dx \tag{11}$$

where the temperature distribution in the constant heat flux case is given by

$$T_a = T_{a,in} + \frac{6q''}{\Pr k_a \mathrm{Re}_{Dp}}x \tag{12}$$

It is worth mentioning that the same friction factor and Nusselt number relationships were used in the constant wall temperature and constant wall heat flux cases.

### 2.3 Computational Implementation and Closure Relationships

A computer program was writen on the EES platform (Klein, 2010) in order to perform the numerical integration of eqs. (7) and (11). Due to their predictions of the PFT heat exchanger experimental data with root mean square errors smaller than 1% (heat transfer) and 3% (pressure drop) (Pussoli *et al.*, 2012), the correlations of Handley and Heggs (1968) and Montillet *et al.* (2007) for the Nusselt number and friction factor were chosen. These are given by

$$\mathrm{Nu}_{Dp} = \frac{0.255}{\varepsilon}\Pr^{1/3}\mathrm{Re}_{Dp}^{2/3} \tag{13}$$

$$f = a\left(\frac{D}{D_p}\right)^{0.2}\left\{\frac{1000}{\mathrm{Re}_{Dp}\left(1-\varepsilon\right)} + \frac{60}{\left[\mathrm{Re}_{Dp}\left(1-\varepsilon\right)\right]^{0.5}} + 12\right\} \tag{14}$$

where $a$ is equal to 0.050 since the porosity, $\varepsilon$, is larger than 0.4 (Montillet *et al.*, 2007). $D$ is the equivalent diameter of the air-side passage. In addition to the porosity, the particle-based Reynolds number and the particle equivalent diameter were chosen as independent variables in the optimization exercise. These are defined as

$$\mathrm{Re}_{D_p} = \frac{U_D D_p}{\nu_a\left(1-\varepsilon\right)} \tag{15}$$

$$D_p = \frac{6V_s}{A} \tag{16}$$

## 3. RESULTS

Results were generated for the three PEC proposed by Webb and Kim (2005): *Fixed Geometry*, **FG** (when the face area and the heat exchanger length are kept fixed during the optimization), *Fixed Face Area*, **FA** (when the face area

is held constant, but the heat exchanger length is free to vary), and *Variable Geometry*, **VG** (when both the face area and the heat exchanger length are free to vary). Table 1 summarizes the cases evaluated in the present study, where the values of the parameters are similar to those investigated experimentally (Pussoli *et al.*, 2012). **CT** and **CH** stand for constant wall temperature and constant heat flux, respectively. The air inlet temperature needed to compute the physical properties is assumed equal to 0°C for all cases. The overall surface efficiency was assumed constant since no knowledge of the actual fin structure or dimensions is needed in order to perform the optimization analysis. Moreover, as $\eta_o$ is only moderately affected by the operating conditions (Pussoli *et al.*, 2012), this assumption seems plausible given the other simplifications already made in this conceptual evaluation of the PFT heat exchanger.

**Table 1:** Parameters and constraints of the optimization analysis.

| PEC | Heat transfer rate (W) | Overall surface efficiency (-) | Face area ($m^2$) | Heat exchanger length (m) | Particle diameter (m) | Porosity (-) | Air mass flow rate (kg/s) | Air-side surface area ($m^2$) |
|---|---|---|---|---|---|---|---|---|
| **FG-CT-1** | 300 | 0.8 | 0.008 | 0.1123 | Variable | 0.85 | Output | Output |
| **FG-CT-2** | 300 | 0.8 | 0.008 | 0.1123 | 0.0015 | Variable | Output | Output |
| **FG-CH** | 300 | 0.8 | 0.008 | 0.1123 | Variable | 0.85 | Output | Output |
| **FA-CT** | 300 | 0.8 | 0.008 | Output | 0.002 | 0.85 | 0.01 | Output |
| **FA-CH** | 300 | 0.8 | 0.008 | Output | 0.002 | 0.85 | 0.01 | Output |
| **VG-CT** | 300 | 0.8 | Output | Output | 0.002 | 0.85 | 0.01 | 0.8086 |
| **VG-CH** | 300 | 0.8 | Output | Output | 0.002 | 0.85 | 0.01 | 0.8086 |

### 3.1 Fixed Geometry

The results for the **FG-CT-1** case are shown in Fig. 3. For each $D_p$ value between 1 and 5 mm, there is a particular $Re_{Dp}$ that yields a minimum total entropy generation rate, which is the sum of individual rates due to heat transfer and pressure drop. The value of this minimum rate $Re_{Dp}$ increases with the particle diameter. Here, an increase in $D_p$ is only possible if the air-side surface area decreases. In practice, this can be achieved by reducing the length and increasing the thickness of the smaller fin arrangements in such a way that the solid volume remains constant. For a given value of $Re_{Dp}$, increasing the particle diameter means that the superficial air velocity must decrease and, for a fixed face area, the resulting decrease in mass flow rate causes an increase in the outlet air temperature. Since the heat transfer rate is a constraint, the upshot is that the internal fluid temperature must increase accordingly, which contributes to raising the rate of entropy generation due to heat transfer across a finite temperature difference.

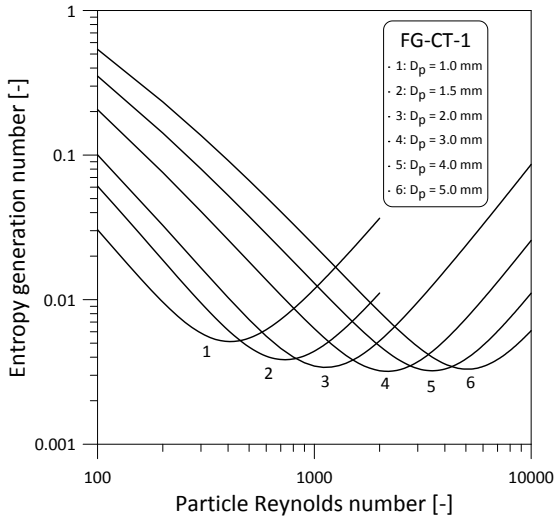


**Figure 3:** $N_S$ results for the **FG-CT-1** case.

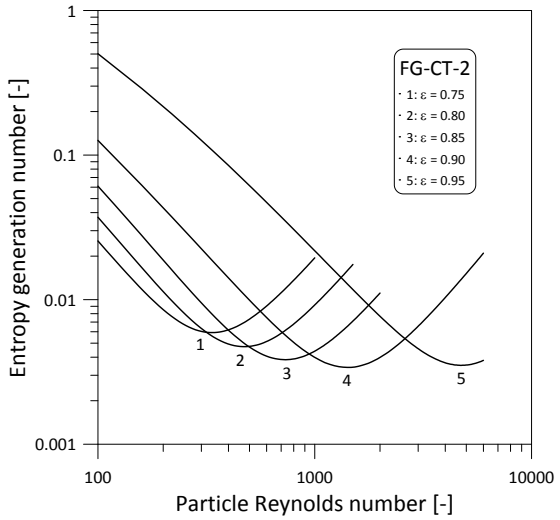


**Figure 4:** $N_S$ results for the **FG-CT-2** case.

Figure 4 shows the results for case **FG-CT-2**. With the overall dimensions and $D_p$ kept fixed, an increase in porosity is such that the associated reduction in the solid volume must be accompanied by a decrease in the surface area, since $D_p$ must be kept constant. Analogous to the **FG-CT-1** case, for a given $Re_{Dp}$, an increase in porosity leads to a reduction of the superficial velocity (and mass flow rate). Thus, if $Re_{Dp}$ is less than the one linked to the minimum $N_S$, an increase in the rate of entropy generation due to finite temperature difference heat transfer is observed because the internal fluid temperature must increase so as to meet the fixed heat transfer rate constraint.

Figure 5 illustrates the existence of a global minimum $N_S$ for the **FG-CT-1** case. A similar plot can be produced for the **FG-CT-2** case by having the porosity in the abscissas. As can be seen, the slope of the curve is less pronounced for values of $D_p$ larger than that associated with the overall minimum $N_S$ (approximately 3 mm). This finding can be combined with the result for the air-side pumping power (see Fig. 6), which also has a global minimum, to determine the best range of operating conditions and/or geometry of the PFT heat exchanger.

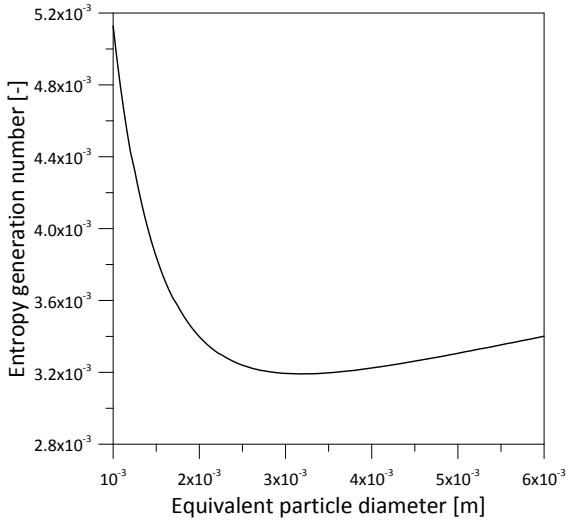


**Figure 5:** Global minimum for the **FG-CT-1** case.

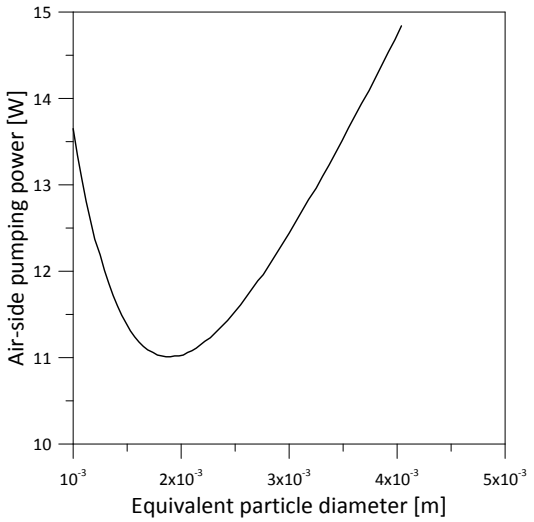


**Figure 6:** Air-side pumping power behavior for the **FG-CT-1** case.

The results for the **FG-CH** case are shown in Figs. 7 and 8. As the particle diameter increases, the surface area must decrease to maintain the porosity constraint. Because the heat transfer rate is also constrained, the heat flux must increase accordingly. Besides, the increase in $D_p$ is also followed by a reduction in superficial velocity for a given $Re_{Dp}$. Therefore, as in the **FG-CT** cases, Fig. 7 shows that increasing $D_p$ causes an increase in the rate of entropy generation due to heat transfer, which may contribute to increasing the total entropy generation rate if the particle Reynolds number is lower than that associated with the minimum $N_S$. Figure 8 shows that a global minimum also exists for the **FG-CH** case, although it is much less sharper than in the constant temperature cases.

### 3.2 Fixed Face Area

In the **FA-CT** and **FA-CH** cases, the mass flow rate is kept fixed and the optimum heat exchanger length can be defined based on the trade-off in entropy generation rate due to heat transfer across a finite temperature difference between the streams and air-side pressure drop. A typical application of the **FA-CT** PEC is the component-level optimization of evaporators for domestic and light commercial refrigerators and freezers, where the cooling capacity may be seen as a design constraint and the face area is fixed due to cabinet space restrictions and positioning of the fan relative to the evaporator.

Figures 9 and 10 show the results obtained for the **FA-CT** case. As can be seen in Fig. 9, the minimum $N_S$ takes place when the heat exchanger length is 0.181 m. Since the mass flow rate is also kept fixed, both $Re_{Dp}$ and the superficial air velocity remain constant. As the heat exchanger length increases, the air temperature decreases because of the associated increase in surface area, which as a whole contributes to decreasing the finite temperature heat transfer contribution to the entropy generation rate (see Fig. 10). Nevertheless, a minimum $N_S$ exists because of the pressure drop contribution, which increases linearly with length. In the **FA-CH** case (Figs. 11 and 12), a similar

behavior is observed, but the minimum $N_S$ occurs at a heat exchanger length of 0.266 m. In this case, a constant heat transfer rate is guaranteed by a decrease in the local heat flux as the heat exchanger length increases. In this way, the temperature difference between the air and the wall decreases as a function of the heat exchanger length.

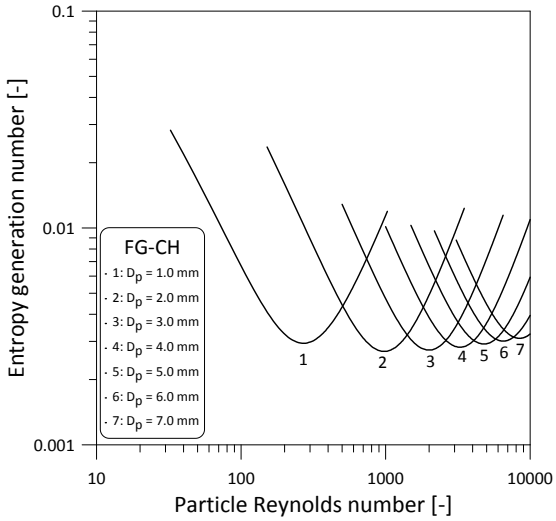


**Figure 7:** $N_S$ results for the **FG-CH** case.

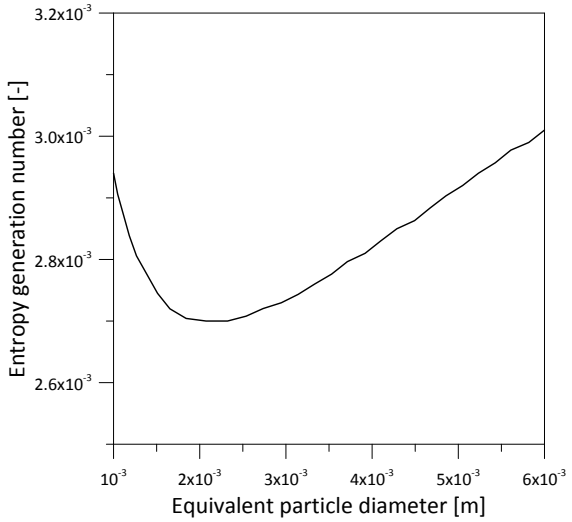


**Figure 8:** Global minimum for the **FG-CH** case.

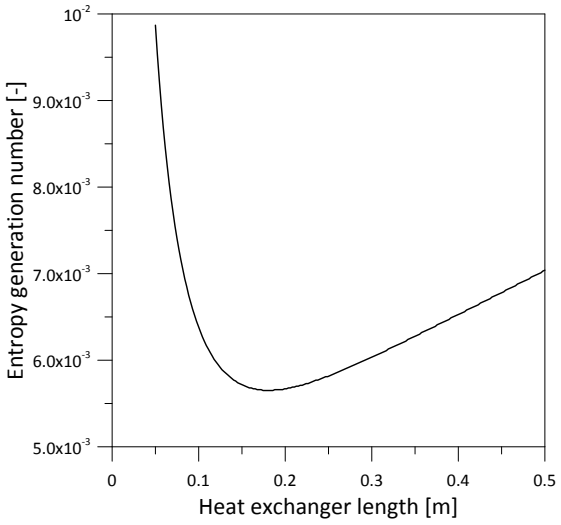


**Figure 9:** $N_S$ results for the **FA-CT** case.

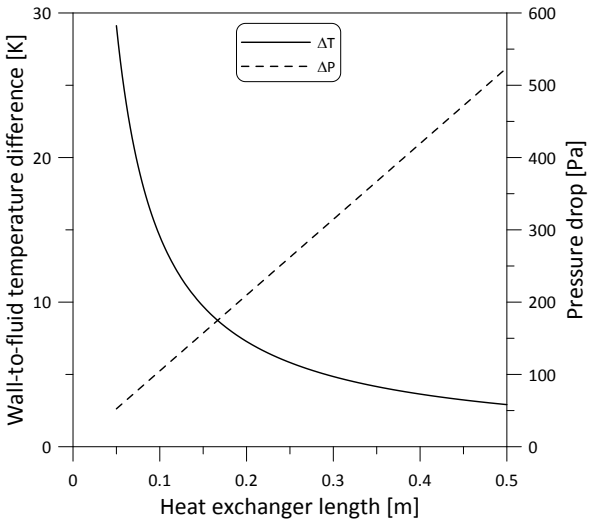


**Figure 10:** Temperature difference and pressure drop results for the **FA-CT** case.

### 3.3 Variable Geometry

This criterion is applicable when changes in the overall dimensions of the heat exchanger are allowed. In the present analysis, it was necessary to constrain, in addition to the heat transfer rate, the total surface area of the heat exchanger (tubes and fins), as can be seen in Table 1. This guarantees that the heat exchanger length and the face area are interdependent and, by changing these variables over an appropriate range, the minimum entropy generation rate can be determined.

In the **VG-CT** case shown in Figs. 13 and 14, the minimum $N_S$ is achieved with a heat exchanger length of 0.137 m and a face area of 0.0132 $m^2$. As the heat exchanger length is increased, the face area must be reduced in order to

satisfy the surface area, porosity and particle diameter constraints. This reduction in face area is accompanied by an increase in the air superficial velocity and $Re_{Dp}$ (and local heat transfer coefficient) because the mass flow rate is also a constraint. This contributes to decreasing the temperature difference between the streams and, consequently, the rate of entropy generation due to heat transfer. However, again, as the heat exchanger length increases and the face area decreases, the associated increase in air superficial velocity and pressure gradient contributes to increasing the pressure drop and its contribution to the entropy generation rate.

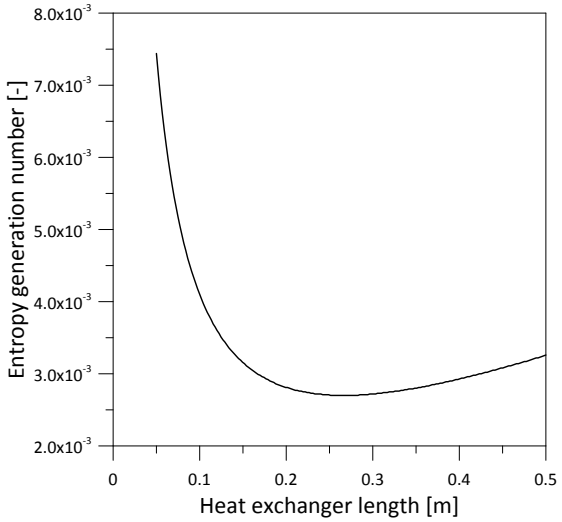


**Figure 11:** $N_S$ results for the **FA-CH** case.

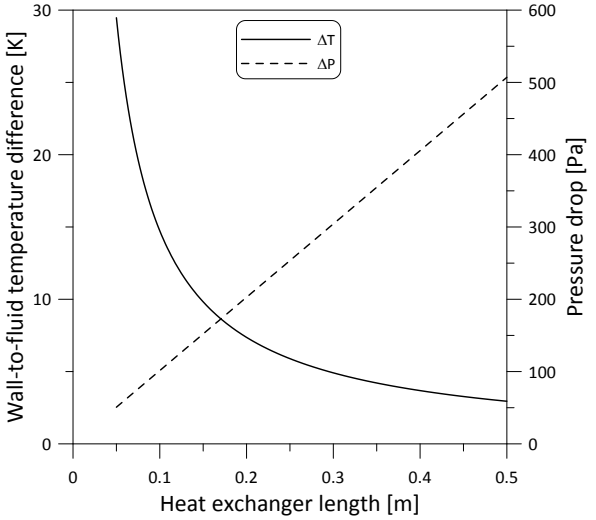


**Figure 12:** Temperature difference and pressure drop results for the **FA-CH** case.

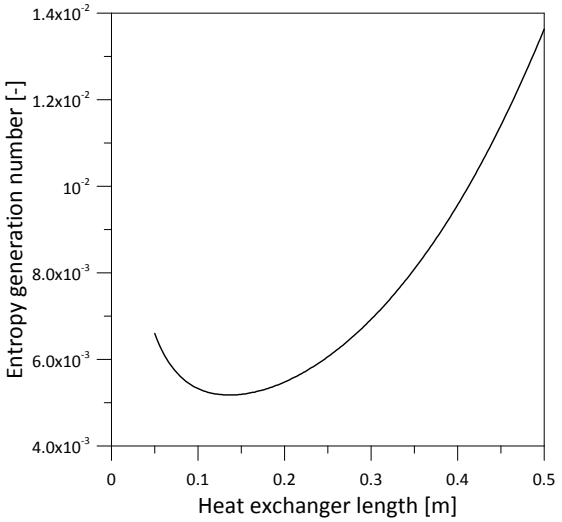


**Figure 13:** $N_S$ results for the **VG-CT** case.

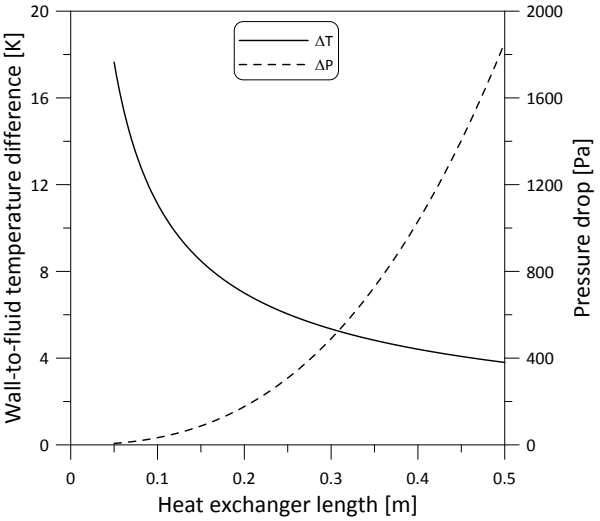


**Figure 14:** Temperature difference and pressure drop results for the **VG-CT** case.

For the **VG-CH** case shown in Figs. 15 and 16, the minimum entropy generation number occurs for a heat exchanger length of 0.1654 m and a face area of 0.0102 $m^2$. As in the **VG-CT** case, the increase in the heat exchanger length reduces the face area and augments the air velocity. The main feature of the **VG-CH** case is that, irrespectively of the length-face area combination, the local heat flux will always remain unchanged. In no other situation evaluated in the present work, the heat flux was independent of the other constraints.

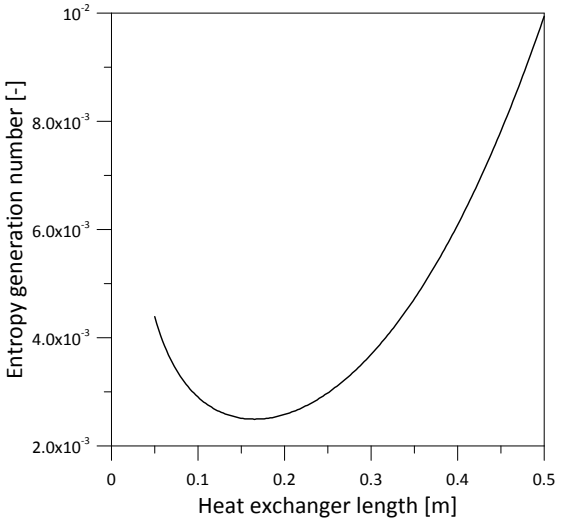


**Figure 15:** $N_S$ results for the **VG-CH** case.

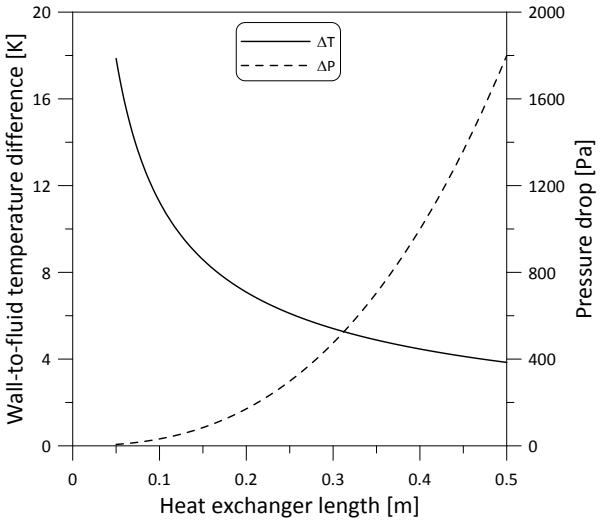


**Figure 16:** Temperature difference and pressure drop results for the **VG-CH** case.

## 4. CONCLUSIONS

An extensive EGM-based optimization analysis of the PFT extended surface geometry has been conducted in this paper. The analysis made use of the fixed geometry (**FG**), fixed face area (**FA**) and variable geometry (**VG**) PEC of Webb and Kim (2005) for both the constant wall temperature and constant heat flux boundary conditions. Due to the large number of geometric variables involved in the PFT heat exchanger, the analysis was focused on the three main dimensionless parameters associated with the fluid flow and heat transfer in the porous medium, i.e., porosity, equivalent particle diameter and particle-based Reynolds number. Closure relationships for the interstitial Nusselt number and friction factor needed in the analysis were those due to Handley and Heggs (1968) and Montillet *et al.* (2007) because of their satisfactory performance in correlating the heat transfer and pressure drop experimental data in real PFT heat exchanger prototypes (Pussoli *et al.*, 2012).

For a fixed heat transfer rate (cooling capacity) of 300 W, which is typical of light commercial refrigeration applications, and other constraints that depended on the PEC under analysis (**FG, FA** or **VG**), it was possible to achieve a combination of independent dimensionless parameters that provided a minimum entropy generation rate for all cases evaluated.

## NOMENCLATURE

| | | |
|---|---|---|
| $A$ | surface area | ($m^2$) |
| $A_c$ | cross-section area | ($m^2$) |
| $c_p$ | specific heat capacity | (J/kg.K) |
| $D_p$ | equivalent particle diameter | (m) |
| $f$ | friction factor | (–) |
| $\bar{h}$ | average convection coefficient | ($W/m^2.K$) |
| $k$ | thermal conductivity | (W/m.K) |
| $L$ | length | (m) |
| $\dot{m}$ | mass flow rate | (kg/s) |
| $N_S$ | entropy generation number | (–) |
| Nu | Nusselt number | (–) |
| $P$ | pressure | (Pa) |
| Pr | Prandtl number | (–) |

**Subscripts**

| | |
|---|---|
| *a* | air |
| *gen* | generation |
| *s* | solid |
| *w* | wall |

| | | |
|---|---|---|
| $q'$ | heat rate per unit length | (W/m) |
| $q''$ | heat flux | (W/m$^2$) |
| Re | Reynolds number | (–) |
| St | Stanton number | (–) |
| $\dot{S}$ | entropy generation rate | (W/K) |
| $T$ | temperature | (K) |
| $x$ | distance | (m) |
| $U_D$ | Darcean (superficial) velocity | (m/s) |
| $V$ | volume | (m$^3$) |

**Greek**

| | | |
|---|---|---|
| $\varepsilon$ | porosity | (–) |
| $\eta_o$ | overall surface efficiency | (–) |
| $\nu$ | kinematic viscosity | (m$^2$/s) |
| $\rho$ | density | (kg/m$^3$) |

## REFERENCES


Wang, C-C., 2000, Technology Review - A Survey of Recent Patents of Fin-and-Tube Heat Exchangers, J. Enhanced Heat Transfer, vol. 7, p. 333-345.

Wang, C-C., 2010, A Survey of Recent Patents on Fin-And-Tube Heat Exchangers from 2001 to 2009, *Int. J. Air-Cond. Refrig.*, vol. 18, p. 1-13.

Wu, H., Ma, D., Kaviany, M., 2007, Peripheral Fins for Blockage Robustness, *Int. J. Heat Mass Transfer*, vol. 50, p. 2514-2520.

Pussoli, B.F., Barbosa Jr., J.R., da Silva, L.W., Kaviany, M., 2012, Heat Transfer and Pressure Drop Characteristics of Peripheral-Finned Tube Heat Exchangers, *Int. J. Heat Mass Transfer*, vol. 55, p. 2835–2843.

Shah, R.K., Sekulic, D., 2003, *Fundamentals of Heat Exchanger Design*, Wiley, New York, 750 p.

Webb, R.L., Kim, N-H., 2005, *Principles of Enhanced Heat Transfer*, 2nd Ed., Taylor and Francis, New York, 795 p.

Yilmaz, M., Karsli, S., Sara, O.N., 2001, Performance Evaluation Criteria for Heat Exchangers Based on Second Law Analysis, *Exergy Int.*, vol. 1, p. 278–294.

Yilmaz, M., Comakli, O., Yapici, S., Sara, O.N., 2005, Performance Evaluation Criteria for Heat Exchangers Based on First Law Analysis, *J. Enhanced Heat Transfer*, vol. 12, p. 121–157.

Zimparov, V., 2000, Extended Performance Evaluation Criteria for Enhanced Heat Transfer Surfaces: Heat Transfer Through Ducts with Constant Wall Temperature, *Int. J. Heat Mass Transfer*, vol. 43, p. 3137-3155.

Zimparov, V., 2001, Extended Performance Evaluation Criteria for Enhanced Heat Transfer Surfaces: Heat Transfer Through Ducts with Constant Heat Flux, *Int. J. Heat Mass Transfer*, vol. 44, p. 169-180.

Bejan, A., 1982, Entropy Generation Through Heat and Fluid Flow, Wiley, New York, 248 p.

Hesselgreaves, J.E., 2000, Rationalization of Second Law Analysis of Heat Exchangers, *Int. J. Heat Mass Transfer*, vol. 43, p. 4189–4204.

Klein, S.A., 2010, *Engineering Equation Solver*, Professional version V8.528.

Kaviany, M., 2011, *Essentials of Heat Transfer*, Cambridge University Press, New York, 2011, 752 p.

Montillet, A., Akkari, E., Comiti, J., 2007, About a Correlating Equation for Predicting Pressure Drops Through Packed Beds of Spheres in a Large Range of Reynolds Numbers, *Chem. Eng. Process.*, vol. 46, p. 329-333.

Handley, D., Heggs, P.J., 1968, Momentum and Heat Transfer Mechanisms in Regular Shaped Packings, *Trans. IChemE*, vol. 46, paper T251.


## ACKNOWLEDGEMENTS

The material presented in this paper is a result of a long-standing technical-scientific partnership between UFSC and Embraco. Financial support from FINEP and CNPq through grant No. 573581/2008-8 (National Institute of Science and Technology in Cooling and Thermophysics) is duly acknowledged.